Engineering Transactions, **70**(3): 221–238, 2022, doi: 10.24423/EngTrans.2038.20220801
Institute of Fundamental Technological Research Polish Academy of Sciences (IPPT PAN)
Université de Lorraine • Poznan University of Technology

Research Paper

Another Six-Node Triangular Element for Structural Analysis

Lan HOANG THAT TON

Department of Civil Engineering, Ho Chi Minh City University of Architecture
Ho Chi Minh, Vietnam; e-mail: tltechonlinesom@gmail.com

A six-node triangular element is presented in this paper for structural analysis. With this approach, the approximation functions of the interpolation strategy are given by using the double interpolation procedure, which includes nodal values as well as averaged nodal gradients. The numerical results are, therefore, achieved following the proposed element. The efficiency of this element and its comparison is described by some fundamental examples. Better numerical solutions and smoother distributions of stresses not achieved by the standard elements will be provided when using this element. The computational time is also presented to overview the pros and cons of the proposed element. In fact, the new element's computational time is higher than that based on the standard element because of the double interpolation procedure, but one does not need post-processing of any smoothing operation.

Key words: finite element method; double interpolation procedure; six-node triangular element.

1. Introduction

Proper design processes of structures are often expensive. Numerical simulations have become very popular and have emerged rapidly around the world. Numerous important engineering structures, such as storage tanks, pressurized aircraft fuselages, pipelines, ship hulls, and so on, are carefully designed. The exact numerical model of the structure is still a challenge to the scientific community of computational mechanics. Many analytical, semi-analytical, experimental, and numerical methods have been presented over the years. Based on the numerical methods, it is easy to realize that the finite element method (FEM) is an effective tool because of its wide application in solving many technical problems. Besides, several developments of new or improved numerical techniques were introduced to resolve the existing disadvantages of the traditional methods. Among these developments are the extended finite element method (XFEM) based on the FEM, which was specially designed for treating discontinuities [1, 2], the meshless method (MM) that does not require a connection between nodes of the simulation domain, i.e., a mesh, but it is instead based on interaction of each node with all its neighbors [3], the smoothed finite element method (SFEM) developed by combining MM with FEM [4–6], the isogeometric analysis (IGA) – a computational approach that offers the possibility of integrating finite element analysis (FEA) into conventional NURBS-based CAD design tools [7–11], FEM based on the C0-HSDT to use lower-order elements [12], FEM related to Chebyshev polynomials for analysis of plate and shell structures [13–15], the twice-interpolation finite element method for solid mechanics problems [16, 17], etc. In this paper, the author presents a six-node triangular finite element based on the double interpolation procedure with smooth nodal stresses that can overcome the difficulties in the standard FEM. Besides advantages, FEM also has some disadvantages, such as the discontinuity of gradients of field variables among elements. In application, the post-processing procedure is often required to obtain the smoothing operation to the nodal stress. In recent years, Zheng *et al.* [16] presented an improved triangular element for elastostatic problems related to the new concept of the double interpolation procedure. This element with various desirable features, such as the continuous nodal stress and higher accuracy of the solutions, is not available in the standard elements. The main idea of the double interpolation procedure is based on the approximation functions that control not only the nodal values but also the averaged nodal gradients as interpolation conditions, see Zheng *et al.* [16] for more details. Nevertheless, this procedure is mainly applied to formulate a trial solution and its continuous derivatives across inter-element boundaries. The stress generated while using this procedure can be smoothed over each domain of the element to improve the solution accuracy without the post-processing process. Another important issue to be noted is that the double interpolation procedure does not change the total number of degrees of freedom of the whole system. The main objective of this study is to introduce a six-node triangular finite element based on the double interpolation procedure for structural analysis with all the above advantages. In the near future, the proposed element will be modified to accurately model singular stress fields near crack tips. The results calculated by the proposed element are validated against reference solutions.

This paper is organized into four sections. In Sec. 2, a formulation of this novel element for structures is presented in which the construction of the shape functions and their properties are recommended. Several examples are subsequently presented in Sec. 3. The author ends this article with some concluding remarks in the last section.

2. Formulation of a six-node triangular element

In this section, the construction of the novel six-node triangular element shape functions and their properties are briefly given. Point $\mathbf{x}$ (x, y) is in the domain of this element with six nodes i, j, k, m, n, p, as schematically shown in Fig. 1.

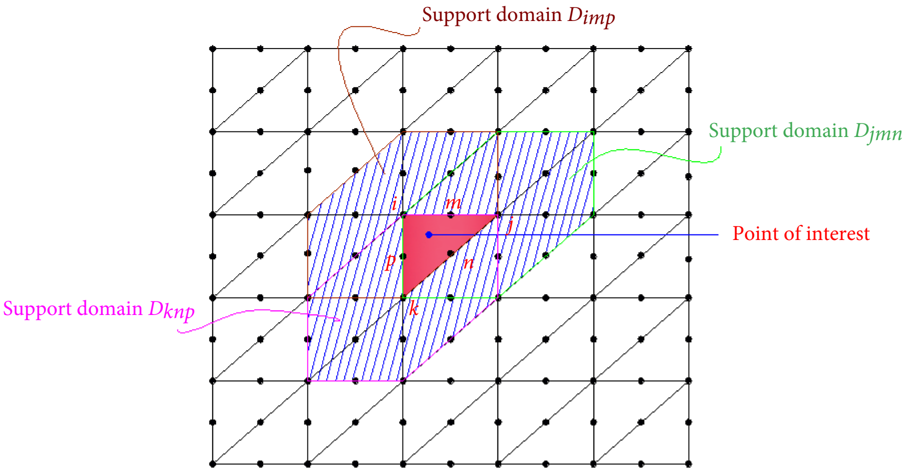

FIG. 1. A six-node triangular element in 2D with the double interpolation procedure and its support domain.

D_{imp}, D_{jmn} and D_{knp} denote elements that share nodes i, j, k, m, n, and p. All nodes of elements D_{imp}, D_{jmn} and D_{knp} are called the supporting nodes of point $\mathbf{x}$ in this novel six-node triangular element. This leads to the support domain for point $\mathbf{x}$ of this element being larger than the support domain of standard FEM. The trial solution at point $\mathbf{x}$ is then shown by:

$$u^h(x) = \sum_{l=1}^{n_{sp}} \widetilde{N}_l(\mathbf{x}) d_l = \widetilde{\mathbf{N}}(\mathbf{x})\mathbf{d}. \tag{2.1}$$

In Eq. (2.1), the double interpolation shape function $\widetilde{N}_l$ is recommended

$$\begin{aligned} \widetilde{N}_l = {} & \underbrace{\Xi_i N_l^{[i]} + \Xi_{ix} \overline{N}_{l,x}^{[i]} + \Xi_{iy} \overline{N}_{l,y}^{[i]}}_{node\ \ i} + \underbrace{\Xi_j N_l^{[j]} + \Xi_{jx} \overline{N}_{l,x}^{[j]} + \Xi_{jy} \overline{N}_{l,y}^{[j]}}_{node\ \ j} \\ & + \underbrace{\Xi_k N_l^{[k]} + \Xi_{kx} \overline{N}_{l,x}^{[k]} + \Xi_{ky} \overline{N}_{l,y}^{[k]}}_{node\ \ k} + \underbrace{\Xi_m N_l^{[m]} + \Xi_{mx} \overline{N}_{l,x}^{[m]} + \Xi_{my} \overline{N}_{l,y}^{[m]}}_{node\ \ m} \\ & + \underbrace{\Xi_n N_l^{[n]} + \Xi_{nx} \overline{N}_{l,x}^{[n]} + \Xi_{ny} \overline{N}_{l,y}^{[n]}}_{node\ \ n} + \underbrace{\Xi_p N_l^{[p]} + \Xi_{px} \overline{N}_{l,x}^{[p]} + \Xi_{py} \overline{N}_{l,y}^{[p]}}_{node\ \ p} \end{aligned} \tag{2.2}$$

in which d_f and $N_f^{[i]}$ are called the nodal displacement vector and the shape function related to node i, respectively. Furthermore, n_{sp} is the total number of the supporting nodes related to point $\mathbf{x}$. At node i, the average derivative of the shape functions is presented below and the same is built for other nodes:

$$\overline{N}_{l,x}^{[i]} = \sum_{e \in D_{imp}} \left(\omega_e N_{l,x}^{[i][e]}\right), \qquad \overline{N}_{l,y}^{[i]} = \sum_{e \in D_{imp}} \left(\omega_e N_{l,y}^{[i][e]}\right). \tag{2.3}$$

In Eq. (2.3), the term $N_{l,x}^{[i][e]}$ is the derivative of $N_l^{[i]}$ calculated in element e, and ω_e is called the weight function of element $e \in D_{imp}$, which is defined by:

$$\omega_e = \frac{\mathit{\Delta}_e}{\sum\limits_{\overline{e} \in D_{imp}} \mathit{\Delta}_{\overline{e}}} \qquad \text{with} \quad e \in D_{imp}, \tag{2.4}$$

and with Δ_e being the area of the element e. In Eq. (2), the functions Ξ_i, Ξ_{ix}, and Ξ_{iy} called the polynomial basis functions associated with the node i must fulfill the following conditions:

$$\begin{aligned}
&\Xi_i\left(\mathbf{x}_l\right) = \delta_{il}, && \Xi_{i,x}\left(\mathbf{x}_l\right) = 0, && \Xi_{i,y}\left(\mathbf{x}_l\right) = 0,\\
&\Xi_{ix}\left(\mathbf{x}_l\right) = 0, && \Xi_{ix,x}\left(\mathbf{x}_l\right) = \delta_{il}, && \Xi_{ix,y}\left(\mathbf{x}_l\right) = 0,\\
&\Xi_{iy}\left(\mathbf{x}_l\right) = 0, && \Xi_{iy,x}\left(\mathbf{x}_l\right) = 0, && \Xi_{iy,y}\left(\mathbf{x}_l\right) = \delta_{il},
\end{aligned} \tag{2.5}$$

where l is from the indices i, j, k, m, n, and p, and

$$\delta_{il} = \begin{cases} 1 & \text{if} \quad i = l, \\ 0 & \text{if} \quad i \neq l. \end{cases} \tag{2.6}$$

Note that the above conditions need to be applied in a similar way to different functions, i.e., Ξ_j, Ξ_{jx}, Ξ_{jy}, Ξ_k, Ξ_{kx}, Ξ_{ky}, Ξ_m, Ξ_{mx}, Ξ_{my}, Ξ_n, Ξ_{nx}, Ξ_{ny}, Ξ_p, Ξ_{px}, and Ξ_{py}. These polynomial basis functions Ξ_i, Ξ_{ix}, and Ξ_{iy} for the proposed element are given by (2.7), (2.8), and (2.9):

$$\begin{aligned}
\Xi_i = {} & A_i + A_i^2 A_j + A_i^2 A_k + A_i^2 A_m + A_i^2 A_n + A_i^2 A_p \\
& - A_i A_j^2 - A_i A_k^2 - A_i A_m^2 - A_i A_n^2 - A_i A_p^2,
\end{aligned} \tag{2.7}$$

$$\begin{aligned}
\Xi_{ix} = {} & -(x_i - x_j)(A_i^2 A_j + 0.5A_i A_j A_k + 0.5A_i A_j A_m + 0.5A_i A_j A_n + 0.5A_i A_j A_p) \\
& - (x_i - x_k)(A_i^2 A_k + 0.5A_i A_k A_j + 0.5A_i A_k A_m + 0.5A_i A_k A_n + 0.5A_i A_k A_p) \\
& - (x_i - x_m)(A_i^2 A_m + 0.5A_i A_m A_j + 0.5A_i A_m A_k + 0.5A_i A_m A_n + 0.5A_i A_m A_p) \\
& - (x_i - x_n)(A_i^2 A_n + 0.5A_i A_n A_j + 0.5A_i A_n A_k + 0.5A_i A_n A_m + 0.5A_i A_n A_p) \\
& - (x_i - x_p)(A_i^2 A_p + 0.5A_i A_p A_j + 0.5A_i A_p A_k + 0.5A_i A_p A_m + 0.5A_i A_p A_n),
\end{aligned} \tag{2.8}$$

(2.9)

$$\begin{aligned}\Xi_{iy} = &-(y_i - y_j)(A_i^2 A_j + 0.5A_iA_jA_k + 0.5A_iA_jA_m + 0.5A_iA_jA_n + 0.5A_iA_jA_p)\\ &- (y_i - y_k)(A_i^2 A_k + 0.5A_iA_kA_j + 0.5A_iA_kA_m + 0.5A_iA_kA_n + 0.5A_iA_kA_p)\\ &- (y_i - y_m)(A_i^2 A_m + 0.5A_iA_mA_j + 0.5A_iA_mA_k + 0.5A_iA_mA_n + 0.5A_iA_mA_p)\\ &- (y_i - y_n)(A_i^2 A_n + 0.5A_iA_nA_j + 0.5A_iA_nA_k + 0.5A_iA_nA_m + 0.5A_iA_nA_p)\\ &- (y_i - y_p)(A_i^2 A_p + 0.5A_iA_pA_j + 0.5A_iA_pA_k + 0.5A_iA_pA_m + 0.5A_iA_pA_n).\end{aligned}$$

In Eqs. (2.7), (2.8), and (2.9), other functions can also be presented in the same way by a circular substitution of indices i, j, k, m, n, and p. In addition, A_i, A_j, A_k, A_m, A_n, and A_p are called the area coordinates of point $\mathbf{x}$ in the six-node triangular element i, j, k, m, n, p, see [16] for more details. It is noted that these shape functions are complete polynomials, satisfy properties of the partition of unity, and carry Kronecker's delta function property. The element stiffness matrix $\mathbf{K_e}$ is then expressed as:

$$\mathbf{K}_e = \int_{\Omega_e} \widetilde{\mathbf{B}}_e^T \mathbf{D} \widetilde{\mathbf{B}}_e \, \mathrm{d}\Omega \tag{2.10}$$

with $\mathbf{D}$ as an elastic tensor and

$$\widetilde{\mathbf{B}}_e = \begin{bmatrix} \widetilde{N}_{1,x} & 0 & \widetilde{N}_{2,x} & 0 & \dots & \widetilde{N}_{l,x} & 0 & \dots & \widetilde{N}_{n_{sp},x} & 0 \\ 0 & \widetilde{N}_{1,y} & 0 & \widetilde{N}_{2,y} & \dots & 0 & \widetilde{N}_{l,y} & \dots & 0 & \widetilde{N}_{n_{sp},y} \\ \widetilde{N}_{1,y} & \widetilde{N}_{1,x} & \widetilde{N}_{2,y} & \widetilde{N}_{2,x} & \dots & \widetilde{N}_{l,y} & \widetilde{N}_{l,x} & \dots & \widetilde{N}_{n_{sp},y} & \widetilde{N}_{n_{sp},x} \end{bmatrix}_{3\times 2n_{sp}}, \tag{2.11}$$

where n_{sp} is called the total number of the supporting nodes due to point $\mathbf{x}$.

3. Fundamental results

3.1. Cantilever beam

A cantilever beam with length $L_1 = 8$ and height $L_2 = 2$ subjected to a parabolic traction $P = -2$ on the right end as given in [18] is presented in Fig. 2. This cantilever beam has a unit thickness and the corresponding analytical solutions of the displacements and stresses for plane stress condition are given by [18]:

$$u_x = -\frac{Py}{6EI}\left[(6L_1 - 3x)x + (2+\nu)\left(y^2 - \frac{L_2^2}{4}\right)\right], \tag{3.1}$$

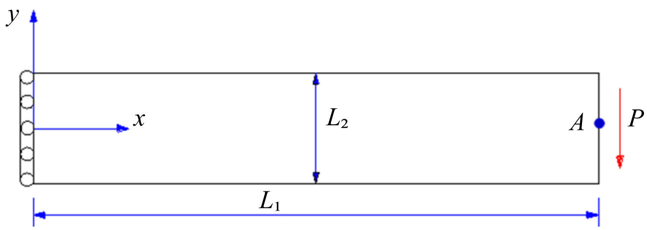

FIG. 2. A cantilever beam subjected to parabolic traction on the right end.

$$u_y = \frac{P}{6EI}\left[3\nu y^2(L_1 - x) + (4+5\nu)\frac{L_2^2 x}{4} + (3L_1 - x)x^2\right], \tag{3.2}$$

$$\sigma_x = -\frac{P(L_1 - x)y}{I}, \tag{3.3}$$

$$\sigma_y = 0, \tag{3.4}$$

$$\tau_{xy} = \frac{P}{2I}\left(\frac{L_2^2}{4} - y^2\right), \tag{3.5}$$

where $I = L_2^3/12$ is calculated as the moment of inertia of the structure.

Only the regular mesh of 16×4 triangular elements with six-node per element is depicted in Fig. 3, but the other meshes of 8×4, 12×4 are also considered and calculate the deflections at point A. The proposed element provides much better results than the standard finite element method with a standard six-node triangular element T6, as shown in Table 1 and Fig. 4.

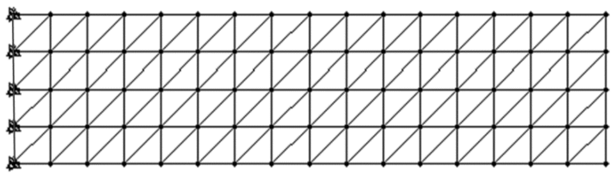

FIG. 3. The discretized mesh using six-node triangular elements.

Table 1. The deflection at point A is based on the standard element T6 and the proposed element.

Deflection at point A	8×4	12×4	16×4
T6	−0.4822	−0.5003	−0.5071
This study	−0.5281	−0.5310	−0.5317
Exact	−0.5330	−0.5330	−0.5330

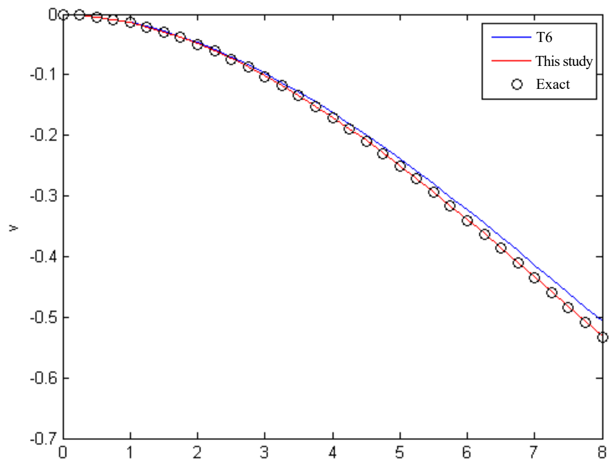

FIG. 4. The deflection along the neutral line with (16 ×4) triangular elements.

Furthermore, the irregular meshes of 8×4, 12×4 and 16×4 are presented in Fig. 5. Again, as shown in Table 2, the results obtained by the proposed element show superiority over the standard six-node element. Besides, Fig. 6 shows that the stress field based on the developed element is very smooth for both regular and irregular meshes though no post-processing is performed.

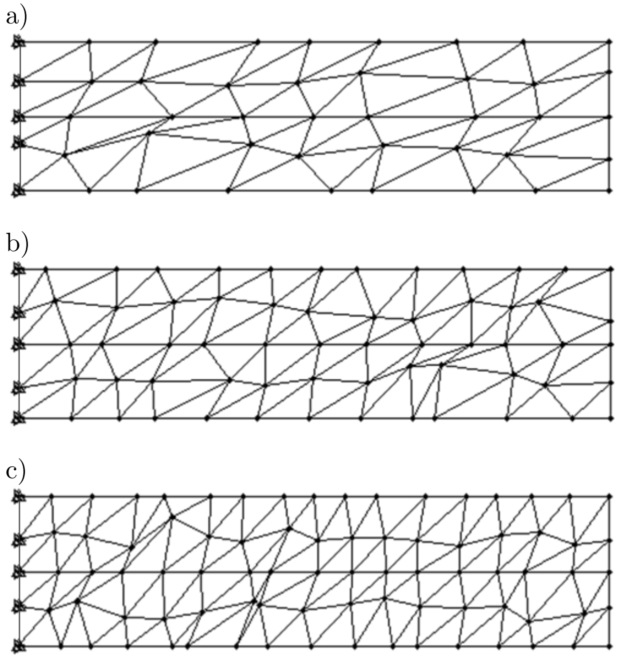

FIG. 5. The distorted meshes using six-node triangular elements: a) 8×4, b) 12×4, c) 16×4.

Table 2. The deflection at point A with irregular meshes.

Deflection at point A	8×4	12×4	16×4
T6	-0.4623	-0.4939	-0.5041
This study	-0.5181	-0.5270	-0.5289
Exact	-0.5330	-0.5330	-0.5330

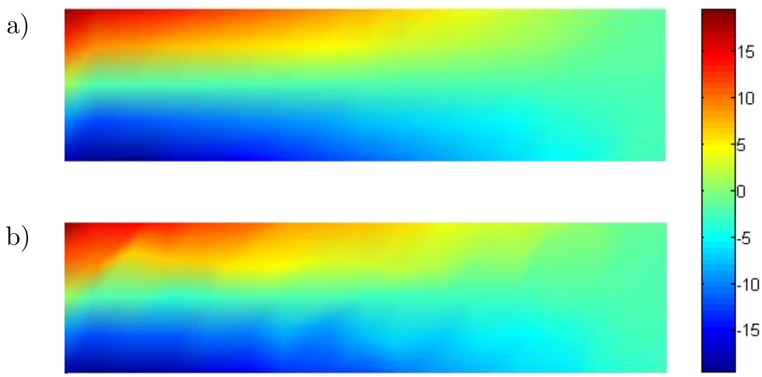

FIG. 6. The stress field related to the proposed element:
a) regular mesh of 16×4, b) irregular mesh of 16×4.

Finally, the computational time needed for the T6 element and the proposed element tested on three different regular meshes of 8×4, 12×4, and 16×4 elements is investigated. The comparison is performed on the same PC of Intel(R) Core(TM) i7 @ 2.80 GHz, 8.GB RAM.

It is observed in Table 3 that the proposed element requires more time than the standard T6 one because of an extra task related to the double interpolation procedure. But one does not need post-processing of any smoothing operation for this element.

Table 3. The computational time.

Time [s]	8×4	12×4	16×4
T6	0.637751	0.643691	0.744800
This study	7.733863	13.414933	20.918070

3.2. An infinite plate with a central circular hole

An infinite plate with a central circular hole of radius r and subjected to a unidirectional tensile loading $q = 1$, as depicted in [18], is studied. Only one-quarter of the plate ($L = 5$, $r = 1$), shown in Fig. 7, is modeled due to

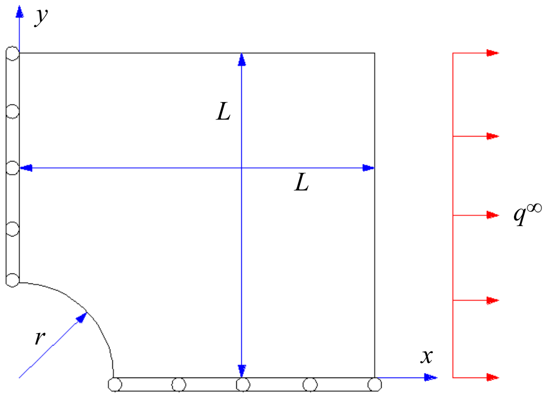

FIG. 7. The quarter model of an infinite plate with a central circular hole.

the two-fold symmetry. The analytical solutions of the displacement and stress fields of the infinite plate are given by [18] for plane stress condition as:

$$u = \frac{q}{4\mu}\left[r_\theta\left[\frac{(\kappa-1)}{2} + \cos(2\theta)\right] + \frac{r^2}{r_\theta}\left[1+(1+\kappa)\cos(2\theta)\right] - \frac{r^4}{r_\theta^3}\cos(2\theta)\right], \tag{3.6}$$

$$v = \frac{q}{4\mu}\left[(1-\kappa)\frac{r^2}{r_\theta} - r_\theta - \frac{r^4}{r_\theta^3}\right]\sin(2\theta), \tag{3.7}$$

$$\sigma_{xx} = q\left\{1 - \frac{r^2}{r_\theta^2}\left[\frac{3}{2}\cos(2\theta) + \cos(4\theta)\right] + \frac{3r^4}{2r_\theta^4}\cos(4\theta)\right\}, \tag{3.8}$$

$$\sigma_{yy} = -q\left\{\frac{r^2}{r_\theta^2}\left[\frac{1}{2}\cos(2\theta) - \cos(4\theta)\right] + \frac{3r^4}{2r_\theta^4}\cos(4\theta)\right\}, \tag{3.9}$$

$$\tau_{xy} = -q\left\{\frac{r^2}{r_\theta^2}\left[\frac{1}{2}\sin(2\theta) + \sin(4\theta)\right] - \frac{3r^4}{2r_\theta^4}\sin(4\theta)\right\}, \tag{3.10}$$

$$\mu = \frac{E}{2(1+\nu)}, \qquad \kappa = \frac{3-\nu}{1+\nu}, \tag{3.11}$$

where r_θ is the distance from the center of the circular hole to the point under consideration, respectively.

Similar to the previous example, the meshes of 8×8 and 16×16 triangular elements with six-node per element are depicted in Fig. 8. The obtained results of the proposed element are not surprising, and as expected, this element outperforms the standard six-node triangular element when the comparisons

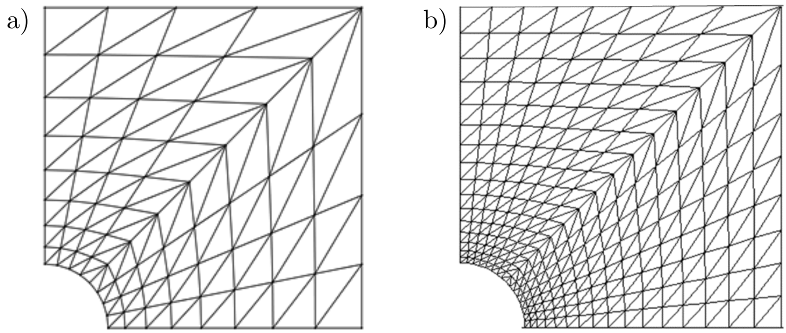

Fig. 8. The discretized mesh using six-node triangular elements: a) 8×8, b) 16×16.

between its results and analytical solutions are made and plotted in Figs. 9–11. Again, Fig. 9 shows that this element provides much smoother stresses than the standard finite element using the same mesh.

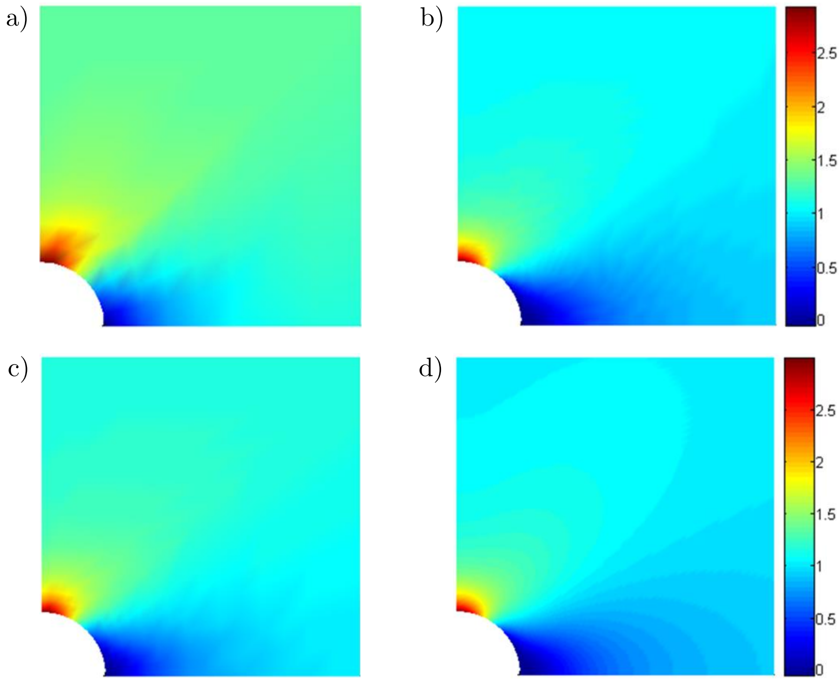

Fig. 9. The stress distribution obtained by the standard six-node triangular element T6 and the proposed element: a) 8×8, T6, b) 8×8, paper, c) 16×16, T6, d) 16×16, paper.

In terms of the verification, Fig. 10 further compares the displacement distributions along the left and bottom boundaries of the quarter plate obtained by the proposed element using a regular mesh of 8×8 elements, and by the T6

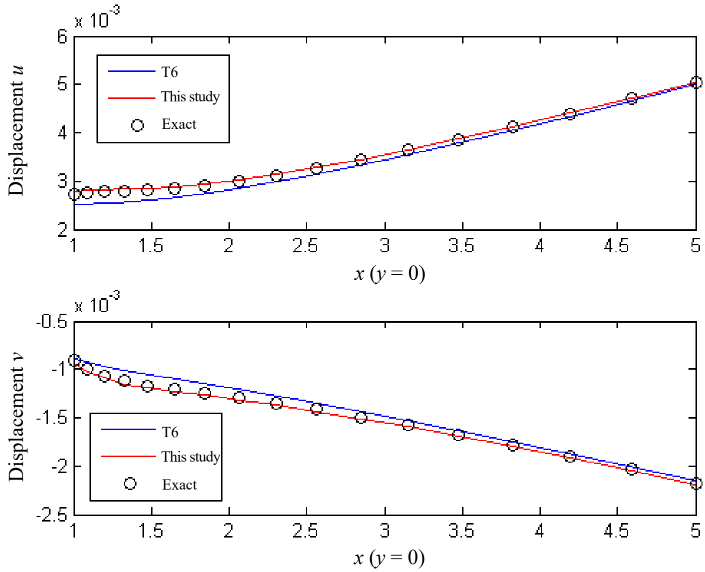

FIG. 10. The displacements along the boundary lines (8×8).

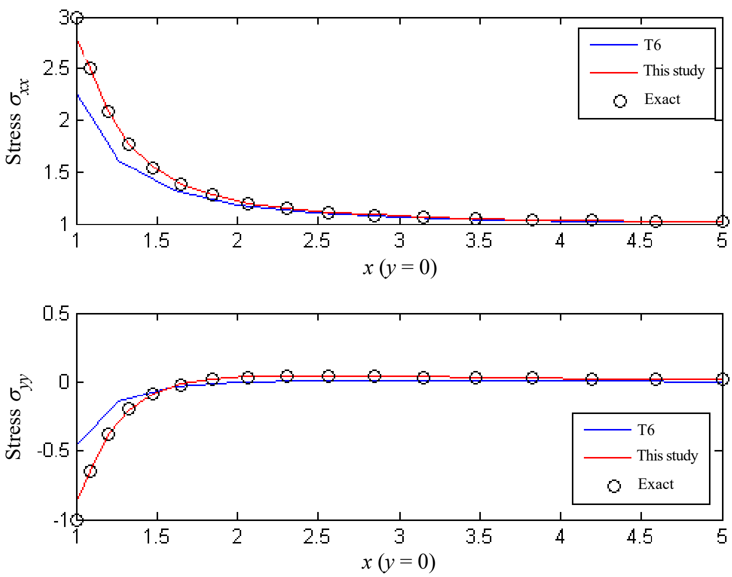

FIG. 11. The stress distributions along the boundary lines (8×8).

element and analytical solutions. It is easy to see that the results obtained by the proposed element completely approximate the analytical solutions and are better than the results of the T6 element. This holds true when comparing the stress distributions along the above boundaries, as shown in Fig. 11.

4. Conclusions

A new numerical method based on a six-node triangular element was introduced for structural analysis. In each case of the study with a different load or geometric shape, the presented numerical results offered higher accuracy than those of the standard element. Furthermore, he applicability of the presented element was clearly shown. Better numerical solutions and smoother distributions of stresses, which are not achieved by the standard elements, will be provided when using this element. The computational time was also studied to review the pros and cons of the proposed element. In fact, this computational time of the proposed six-node element was higher than that based on the standard element because of the double interpolation procedure, but one does not need post-processing of any smoothing operation.

Appendix

Let us consider a six-node triangular element presented in Fig. 1. The functions A_i, A_j, A_k, A_m, A_n, and A_p are given as:

$$A_i = 1 - 3(r+s) + 4rs + 2(r^2 + s^2), \qquad A_j = r(2r-1), \qquad A_k = s(2s-1),$$

$$A_m = 4r(1-r-s), \qquad A_n = 4rs, \qquad A_p = 4s(1-r-s).$$

The derivatives of the above functions are:

$$\begin{Bmatrix} \dfrac{\partial}{\partial r} \\ \dfrac{\partial}{\partial s} \end{Bmatrix} \begin{bmatrix} A_i & A_j & A_k & A_m & A_n & A_p \end{bmatrix}$$

$$= \begin{bmatrix} -3+4r+4s & 4r-1 & 0 & 4-8r-4s & 4s & -4s \\ -3+4s+4r & 0 & 4s-1 & -4r & 4r & 4-4r-8s \end{bmatrix}.$$

The Jacobian matrix and its inverse are described as:

$$\mathbf{J} = \begin{bmatrix} -3+4r+4s & 4r-1 & 0 & 4-8r-4s & 4s & -4s \\ -3+4s+4r & 0 & 4s-1 & -4r & 4r & 4-4r-8s \end{bmatrix} \begin{Bmatrix} x_i & y_i \\ x_j & y_j \\ x_k & y_k \\ x_m & y_m \\ x_n & y_n \\ x_p & y_p \end{Bmatrix},$$

$$\mathbf{J}^{-1} = \frac{1}{\det \mathbf{J}} \begin{bmatrix} J_1 & J_2 \\ J_3 & J_4 \end{bmatrix},$$

$$J_1 = (-3 + 4r + 4s)\, y_i + (4s - 1)\, y_k - 4ry_m + 4ry_n + (4 - 4r - 8s)\, y_p,$$

$$J_2 = -(-3 + 4r + 4s)\, x_i - (4s - 1)\, x_k + 4rx_m - 4rx_n - (4 - 4r - 8s)\, x_p,$$

$$J_3 = -(-3 + 4r + 4s)\, y_i - (4r - 1)\, y_j - (4 - 8r - 4s)\, y_m + 4sy_p - 4sy_n,$$

$$J_4 = (-3 + 4r + 4s)\, x_i + (4r - 1)\, x_j + (4 - 8r - 4s)\, x_m + 4sx_n - 4sx_p.$$

The derivatives of the geometric interpolation functions can be expressed as:

$$\frac{\partial \Xi_i}{\partial A_i} = 1 + 2A_iA_j + 2A_iA_k + 2A_iA_m + 2A_iA_n + 2A_iA_p - A_j^2 - A_k^2 - A_m^2 - A_n^2 - A_p^2,$$

$$\frac{\partial \Xi_i}{\partial A_j} = A_i^2 - 2A_iA_j, \qquad \frac{\partial \Xi_i}{\partial A_k} = A_i^2 - 2A_iA_k, \qquad \frac{\partial \Xi_i}{\partial A_m} = A_i^2 - 2A_iA_m,$$

$$\frac{\partial \Xi_i}{\partial A_n} = A_i^2 - 2A_iA_n, \qquad \frac{\partial \Xi_i}{\partial A_p} = A_i^2 - 2A_iA_p,$$

$$\begin{aligned}\frac{\partial \Xi_{ix}}{\partial A_i} = &-(x_i - x_j)\,(2A_iA_j + 0.5A_jA_k + 0.5A_jA_m + 0.5A_jA_n + 0.5A_jA_p) \\ &-(x_i - x_k)\,(2A_iA_k + 0.5A_kA_j + 0.5A_kA_m + 0.5A_kA_n + 0.5A_kA_p) \\ &-(x_i - x_m)\,(2A_iA_m + 0.5A_mA_j + 0.5A_mA_k + 0.5A_mA_n + 0.5A_mA_p) \\ &-(x_i - x_n)\,(2A_iA_n + 0.5A_nA_j + 0.5A_nA_k + 0.5A_nA_m + 0.5A_nA_p) \\ &-(x_i - x_p)\,(2A_iA_p + 0.5A_pA_j + 0.5A_pA_k + 0.5A_pA_m + 0.5A_pA_n),\end{aligned}$$

$$\begin{aligned}\frac{\partial \Xi_{ix}}{\partial A_j} = &-(x_i - x_j)\left(A_i^2 + 0.5A_iA_k + 0.5A_iA_m + 0.5A_iA_n + 0.5A_iA_p\right) \\ &-(x_i - x_k)\,(0.5A_iA_k) - (x_i - x_m)\,(0.5A_iA_m) - (x_i - x_n)\,(0.5A_iA_n) \\ &-(x_i - x_p)\,(0.5A_iA_p),\end{aligned}$$

$$\begin{aligned}\frac{\partial \Xi_{ix}}{\partial A_k} = &-(x_i - x_j)\,(0.5A_iA_j) \\ &-(x_i - x_k)\left(A_i^2 + 0.5A_iA_j + 0.5A_iA_m + 0.5A_iA_n + 0.5A_iA_p\right) \\ &-(x_i - x_m)\,(0.5A_iA_m) - (x_i - x_n)\,(0.5A_iA_n) - (x_i - x_p)\,(0.5A_iA_p),\end{aligned}$$

$$\begin{aligned}\frac{\partial \Xi_{ix}}{\partial A_m} =& -(x_i - x_j)(0.5A_iA_j) - (x_i - x_k)(0.5A_iA_k)\\ & - (x_i - x_m)\left(A_i^2 + 0.5A_iA_j + 0.5A_iA_k + 0.5A_iA_n + 0.5A_iA_p\right)\\ & - (x_i - x_n)(0.5A_iA_n) - (x_i - x_p)(0.5A_iA_p),\end{aligned}$$

$$\begin{aligned}\frac{\partial \Xi_{ix}}{\partial A_n} =& -(x_i - x_j)(0.5A_iA_j) - (x_i - x_k)(0.5A_iA_k) - (x_i - x_m)(0.5A_iA_m)\\ & - (x_i - x_n)\left(A_i^2 + 0.5A_iA_j + 0.5A_iA_k + 0.5A_iA_m + 0.5A_iA_p\right)\\ & - (x_i - x_p)(0.5A_iA_p),\end{aligned}$$

$$\begin{aligned}\frac{\partial \Xi_{ix}}{\partial A_p} =& -(x_i - x_j)(0.5A_iA_j) - (x_i - x_k)(0.5A_iA_k)\\ & - (x_i - x_m)(0.5A_iA_m) - (x_i - x_n)(0.5A_iA_n)\\ & - (x_i - x_p)\left(A_i^2 + 0.5A_iA_j + 0.5A_iA_k + 0.5A_iA_m + 0.5A_iA_n\right),\end{aligned}$$

$$\begin{aligned}\frac{\partial \Xi_{iy}}{\partial A_i} =& -(y_i - y_j)(2A_iA_j + 0.5A_jA_k + 0.5A_jA_m + 0.5A_jA_n + 0.5A_jA_p)\\ & - (y_i - y_k)(2A_iA_k + 0.5A_kA_j + 0.5A_kA_m + 0.5A_kA_n + 0.5A_kA_p)\\ & - (y_i - y_m)(2A_iA_m + 0.5A_mA_j + 0.5A_mA_k + 0.5A_mA_n + 0.5A_mA_p)\\ & - (y_i - y_n)(2A_iA_n + 0.5A_nA_j + 0.5A_nA_k + 0.5A_nA_m + 0.5A_nA_p)\\ & - (y_i - y_p)(2A_iA_p + 0.5A_pA_j + 0.5A_pA_k + 0.5A_pA_m + 0.5A_pA_n),\end{aligned}$$

$$\begin{aligned}\frac{\partial \Xi_{iy}}{\partial A_j} =& -(y_i - y_j)\left(A_i^2 + 0.5A_iA_k + 0.5A_iA_m + 0.5A_iA_n + 0.5A_iA_p\right)\\ & - (y_i - y_k)(0.5A_iA_k) - (y_i - y_m)(0.5A_iA_m) - (y_i - y_n)(0.5A_iA_n)\\ & - (y_i - y_p)(0.5A_iA_p),\end{aligned}$$

$$\begin{aligned}\frac{\partial \Xi_{iy}}{\partial A_k} =& -(y_i - y_j)(0.5A_iA_j)\\ & - (y_i - y_k)\left(A_i^2 + 0.5A_iA_j + 0.5A_iA_m + 0.5A_iA_n + 0.5A_iA_p\right)\\ & - (y_i - y_m)(0.5A_iA_m) - (y_i - y_n)(0.5A_iA_n) - (y_i - y_p)(0.5A_iA_p),\end{aligned}$$

$$\begin{aligned}\frac{\partial \Xi_{iy}}{\partial A_m} =& -(y_i - y_j)(0.5A_iA_j) - (y_i - y_k)(0.5A_iA_k)\\ & - (y_i - y_m)\left(A_i^2 + 0.5A_iA_j + 0.5A_iA_k + 0.5A_iA_n + 0.5A_iA_p\right)\\ & - (y_i - y_n)(0.5A_iA_n) - (y_i - y_p)(0.5A_iA_p),\end{aligned}$$

$$\begin{aligned}\frac{\partial \Xi_{iy}}{\partial A_n} =& -\left(y_i-y_j\right)\left(0.5A_iA_j\right)-\left(y_i-y_k\right)\left(0.5A_iA_k\right)-\left(y_i-y_m\right)\left(0.5A_iA_m\right)\\ &-\left(y_i-y_n\right)\left(A_i^2+0.5A_iA_j+0.5A_iA_k+0.5A_iA_m+0.5A_iA_p\right)\\ &-\left(y_i-y_p\right)\left(0.5A_iA_p\right),\end{aligned}$$

$$\begin{aligned}\frac{\partial \Xi_{iy}}{\partial A_p} =& -\left(y_i-y_j\right)\left(0.5A_iA_j\right)-\left(y_i-y_k\right)\left(0.5A_iA_k\right)\\ &-\left(y_i-y_m\right)\left(0.5A_iA_m\right)-\left(y_i-y_n\right)\left(0.5A_iA_n\right)\\ &-\left(y_i-y_p\right)\left(A_i^2+0.5A_iA_j+0.5A_iA_k+0.5A_iA_m+0.5A_iA_n\right).\end{aligned}$$

Now, we prove the condition: $\Xi_i\left(x_l\right)=\delta_{il}$. When $l\equiv i$, then $r=0$, $s=0$ and $A_i=1$, $A_j=A_k=A_m=A_n=A_p=0$, substituting them into above equations we obtain $\Xi_i\left(x_i\right)=1$. Similarly, when $l\equiv j$, $l\equiv k$, $l\equiv m$, $l\equiv n$ or $l\equiv p$ we obtain $\Xi_i\left(x_j\right)=0$, $\Xi_i\left(x_k\right)=0$, $\Xi_i\left(x_m\right)=0$, $\Xi_i\left(x_n\right)=0$, and $\Xi_i\left(x_p\right)=0$, respectively.

Next, we prove the conditions: $\Xi_{i,x}\left(x_l\right)=0$ and $\Xi_{i,y}\left(x_l\right)=0$. When $l\equiv i$, then $r=0$, $s=0$, and $A_i=1$, $A_j=A_k=A_m=A_n=A_p=0$. Substituting them into the above equations we have

$$\left\{\begin{array}{c}\dfrac{\partial}{\partial r}\\ \dfrac{\partial}{\partial s}\end{array}\right\}\left[\begin{array}{cccccc}A_i & A_j & A_k & A_m & A_n & A_p\end{array}\right]=\begin{bmatrix}-3 & -1 & 0 & 4 & 0 & 0\\ -3 & 0 & -1 & 0 & 0 & 4\end{bmatrix},$$

$$\mathbf{J}^{-1}=\frac{1}{\det\mathbf{J}}\begin{bmatrix}-3y_i-y_k+4y_p & 3x_i+x_k-4x_p\\ 3y_i+y_j-4y_m & -3x_i-x_j+4x_m\end{bmatrix},$$

$$\begin{aligned}\left\{\begin{array}{c}\dfrac{\partial}{\partial x}\\ \dfrac{\partial}{\partial y}\end{array}\right\}\left[\begin{array}{cccccc}A_i & A_j & A_k & A_m & A_n & A_p\end{array}\right]&=\mathbf{J}^{-1}\left\{\begin{array}{c}\dfrac{\partial}{\partial r}\\ \dfrac{\partial}{\partial s}\end{array}\right\}\left[\begin{array}{cccccc}A_i & A_j & A_k & A_m & A_n & A_p\end{array}\right]\\ &=\frac{1}{\det\mathbf{J}}\begin{bmatrix}-3y_i-y_k+4y_p & 3x_i+x_k-4x_p\\ 3y_i+y_j-4y_m & -3x_i-x_j+4x_m\end{bmatrix}\begin{bmatrix}-3 & -1 & 0 & 4 & 0 & 0\\ -3 & 0 & -1 & 0 & 0 & 4\end{bmatrix}\\ &=\frac{1}{\det\mathbf{J}}\mathbf{X},\end{aligned}$$

$$\frac{\partial \Xi}{\partial A_i}=\frac{\partial \Xi}{\partial A_j}=\frac{\partial \Xi}{\partial A_k}=\frac{\partial \Xi}{\partial A_m}=\frac{\partial \Xi}{\partial A_n}=\frac{\partial \Xi}{\partial A_p}=1,$$

where

$$\mathbf{X}=\begin{bmatrix} 9y_i+3y_k-12y_p-9x_i-3x_k+12x_p & -9y_i-3y_j+12y_m+9x_i+3x_j-12x_m \\ 3y_i+y_k-4y_p & -3y_i-y_j+4y_m \\ -3x_i-x_k+4x_p & 3x_i+x_j-4x_m \\ -12y_i-4y_k+16y_p & 12y_i+4y_j-16y_m \\ 0 & 0 \\ 12x_i+4x_k-16x_p & -12x_i-4x_j+16x_m \end{bmatrix}^{\mathrm{T}}.$$

Then, we finally obtain $\Xi_{i,x}(x_l)=0$, $\Xi_{i,y}(x_l)=0$ as:

$$\Xi_{i,x}(x_i)=\frac{\partial\Xi_i}{\partial x}=\begin{bmatrix} \frac{\partial\Xi_i}{\partial A_i} & \frac{\partial\Xi_i}{\partial A_j} & \frac{\partial\Xi_i}{\partial A_k} & \frac{\partial\Xi_i}{\partial A_m} & \frac{\partial\Xi_i}{\partial A_n} & \frac{\partial\Xi_i}{\partial A_p} \end{bmatrix} \times \left\{ \frac{\partial A_i}{\partial x} \quad \frac{\partial A_j}{\partial x} \quad \frac{\partial A_k}{\partial x} \quad \frac{\partial A_m}{\partial x} \quad \frac{\partial A_n}{\partial x} \quad \frac{\partial A_p}{\partial x} \right\}^{\mathrm{T}}$$

$$=\begin{bmatrix} 1 & 1 & 1 & 1 & 1 & 1 \end{bmatrix}\frac{1}{\det\mathbf{J}}\begin{bmatrix} 9y_i+3y_k-12y_p-9x_i-3x_k+12x_p \\ 3y_i+y_k-4y_p \\ -3x_i-x_k+4x_p \\ -12y_i-4y_k+16y_p \\ 0 \\ 12x_i+4x_k-16x_p \end{bmatrix}=0,$$

$$\Xi_{i,y}(x_i)=\frac{\partial\Xi_i}{\partial y}=\begin{bmatrix} \frac{\partial\Xi_i}{\partial A_i} & \frac{\partial\Xi_i}{\partial A_j} & \frac{\partial\Xi_i}{\partial A_k} & \frac{\partial\Xi_i}{\partial A_m} & \frac{\partial\Xi_i}{\partial A_n} & \frac{\partial\Xi_i}{\partial A_p} \end{bmatrix} \times \left\{ \frac{\partial A_i}{\partial y} \quad \frac{\partial A_j}{\partial y} \quad \frac{\partial A_k}{\partial y} \quad \frac{\partial A_m}{\partial y} \quad \tfrac{\partial A_n}{\partial y} \quad \frac{\partial A_p}{\partial y} \right\}^{\mathrm{T}}$$

$$=\begin{bmatrix} 1 & 1 & 1 & 1 & 1 & 1 \end{bmatrix}\frac{1}{\det\mathbf{J}}\begin{bmatrix} -9y_i-3y_j+12y_m+9x_i+3x_j-12x_m \\ -3y_i-y_j+4y_m \\ 3x_i+x_j-4x_m \\ 12y_i+4y_j-16y_m \\ 0 \\ -12x_i-4x_j+16x_m \end{bmatrix}=0.$$

Other cases can be proved similarly.

Conflicts of interest

The author declares no conflict of interest.

References

1. Kumar S., Singh I.V., Mishra B.K., XFEM simulation of stable crack growth using J–R curve under finite strain plasticity, *International Journal of Mechanics and Materials in Design*, **10**(2): 165–177, 2014, doi: 10.1007/s10999-014-9238-1.

2. Prashant Singh A., Tailor A., Tumrate C. S., Mishra D., Crack growth simulation in a functionally graded material plate with uniformly distributed pores using extended finite element method, *Materials Today: Proceedings*, **60**(1): 602–607, 2022, doi: 10.1016/j.matpr.2022.02.123.

3. Bui Tinh Q., Nguyen Minh N., A novel meshfree model for buckling and vibration analysis of rectangular orthotropic plates, *Structural Engineering and Mechanics*, **39**(4): 579–598, 2011.

4. Ton-That H.L., Nguyen-Van A., A combined strain element in static, frequency and buckling analyses of laminated composite plates and shells, *Periodica Polytechnica Civil Engineering*, **65**(1): 56–71, 2021, doi: 10.3311/PPci.16809.

5. Ton-That H.L., A combined strain element to functionally graded structures in thermal environment, *Acta Polytechnica*, **60**(6): 528–539, 2020, doi: 10.14311/AP.2020.60.0528.

6. Ton-That H.L., Nguyen-Van H., Chau-Dinh T., Static and buckling analyses of stiffened plate/shell structures using the quadrilateral element SQ4C, *Comptes Rendus Mécanique*, **348**(4): 285–305, 2020, doi: 10.5802/crmeca.7.

7. Lai W. *et al.*, 3-D elasto-plastic large deformations: IGA simulation by Bézier extraction of NURBS, *Advances in Engineering Software*, **108**: 68–82, 2017, doi: 10.1016/j.advengsoft.2017.02.011.

8. Patil R.U., Mishra B.R., Singh I.V., Bui T.Q., A new multiscale phase field method to simulate failure in composites, *Advances in Engineering Software*, **126**: 9–33, 2018, doi: 10.1016/j.advengsoft.2018.08.010.

9. Nguyen M.N., Bui T.Q., Yu T., Hirose S., Isogeometric analysis for unsaturated flow problems, *Computers and Geotechnics*, **62**: 257–267, 2014, doi: 10.1016/j.compgeo.2014.08.003.

10. Kim M.-G, Lee G.-H., Lee H., Koo B., Isogeometric analysis for geometrically exact shell elements using Bézier extraction of NURBS with assumed natural strain method, *Thin-Walled Structures*, **172**: 108846, 2022, doi: 10.1016/j.tws.2021.108846.

11. Hu H., Batou A., Ouyang H., An Isogeometric analysis based method for frictional elastic contact problems with randomly rough surfaces, *Computer Methods in Applied Mechanics and Engineering*, **394**: 114865, 2022, doi: 10.1016/j.cma.2022.114865.

12. Ton-That H.L., The linear and nonlinear bending analyses of functionally graded carbon nanotube-reinforced composite plates based on the novel four-node quadrilateral element, *European Journal of Computational Mechanics*, **29**(1): 139–172, 2020, doi: 10.13052/ejcm2642-2085.2915.

13. Dang-Trung H., Yang D.-J., Liu Y.C., Improvements in shear locking and spurious zero energy modes using Chebyshev finite element method, *Journal of Computing and Information Science in Engineering*, **19**(1): 011006, 2018, doi: 10.1115/1.4041829.

14. Liu T., Wang Q., Qin B., Wang A., Free in-plane vibration of plates with arbitrary curvilinear geometry: Spectral-Chebyshev model and experimental study, *Thin-Walled Structures*, **170**: 108628, 2022, doi: 10.1016/j.tws.2021.108628.

15. Ton-That H.L., Nguyen-Van H., Chau-Dinh T., A novel quadrilateral element for analysis of functionally graded porous plates/shells reinforced by graphene platelets, *Archive of Applied Mechanics*, **91**(6): 2435–2466, 2021, doi: 10.1007/s00419-021-01893-6.

16. Zheng C. *et al.*, A novel twice-interpolation finite element method for solid mechanics problems, *Acta Mechanica Sinica*, **26**(2): 265–278, 2010, doi: 10.1007/s10409-009-0265-3.

17. Wu S.C., Zhang W.H., Peng X., Miao B.R., A twice-interpolation finite element method (TFEM) for crack propagation problems, *International Journal of Computational Methods*, **09**(04): 1250055, 2012, doi: 10.1142/S0219876212500557.

18. Timoshenko S.P., Goodier J., *Theory of Elasticity*, 3rd. ed., New York: McGraw-Hill, 1970.

Received March 2, 2022; accepted version May 16, 2022.